Superlattices and Microstructures, Vol. 20, No. 3, 1996

Interface roughness, polar optical phonons, and the valley current of a resonant tunneling diode

R. Lake, G. Klimeck, R. C. Bowen,
C. Fernando, T. Moise, Y. C. Kao
Corporate R&D, Texas Instruments Incorporated, Dallas, Texas 75243, U.S.A.

M. Leng
Erik Jonsson School of Engineering and Computer Science,
The University of Texas at Dallas, Richardson, TX 75083, U.S.A.

(Received 20 May 1996)

Theory, numerical simulations, and experimental measurements of the valley current of a GaAs/AlAs resonant tunneling diode are compared. The effect on the valley current of different interface-roughness correlation models, island sizes, and asymmetric roughness is described. Initially, the valley current increases quadratically with island size. Between 6 and 10 nm there is a crossover and the contribution to the valley current begins to decrease. Asymmetric roughness on normal and inverted interfaces (smooth normal and rough inverted) results in order of magnitude different contributions to the valley current under forward and reverse bias. This asymmetry in the valley current occurs even when the polar optical phonon scattering is taken into account. The polar optical phonon scattering dominates the valley current.

The peak to valley current ratio and correspondent utility of resonant tunneling diodes is ultimately determined by scattering which has been studied using a number of different models and approaches [1–5]. We present a study of interface roughness asymmetry, the effect of different island sizes, and polar optical phonon scattering on the valley current of a GaAs/AlAs resonant tunneling diode (RTD) at T = 4.2 K. We present the first calculations comparing the Gaussian and exponential roughness correlation models. The calculations are compared with the experimental data. A similar study of an InP lattice matched InGaAs/AlAs/InAs RTD was recently reported by Roblin, Potter, and Fathimulla [6]. There is a notable difference in our conclusion. The experimental data and our simulations show that the valley current for the GaAs/AlAs RTD is dominated by polar optical phonon scattering whereas Roblin *et al*. find the valley current to be dominated by interface roughness scattering.

We model interface roughness as a single monolayer of alloy in which the cation species of a given type cluster into islands. The first order term gives the virtual crystal Hamiltonian. The clustering results in a momentum dependence of the autocorrelation function. The model smoothly approaches the usual alloy

0749–6036/96/070279 + 07 $18.00/0

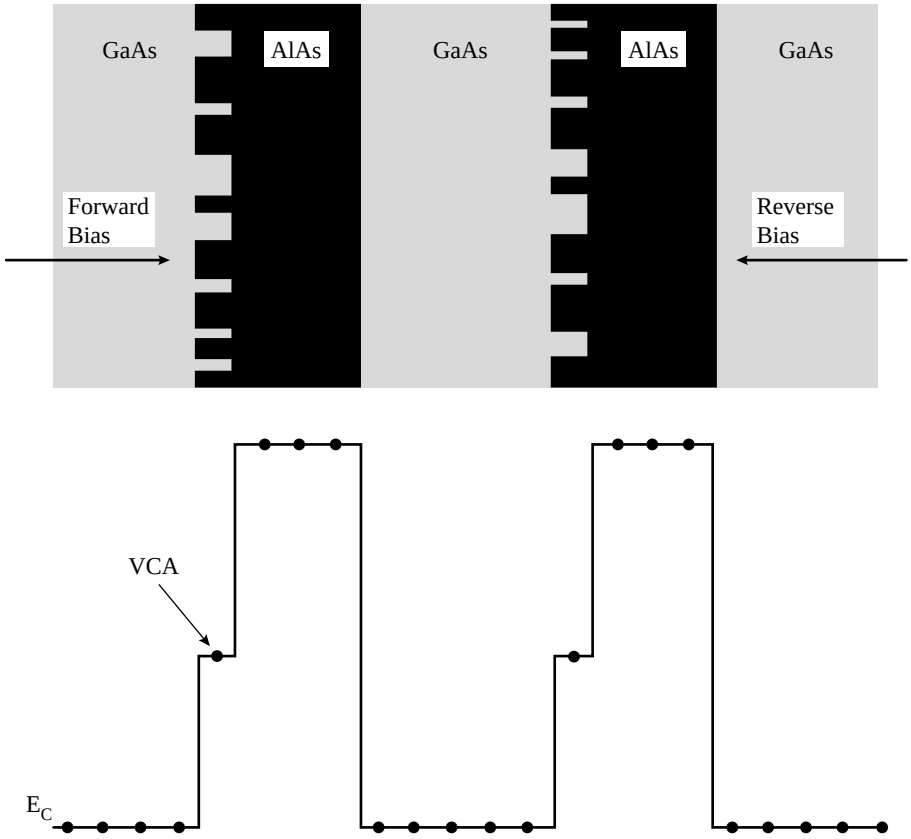

Fig. 1. Illustration of interface roughness in the single band model. The average potential results in a virtual crystal term in the Hamiltonian at the interface layer. Under forward bias, the injected electrons are incident on the rough interfaces.

model as the clustering becomes a homogeneous mixture of the two cation species. This does not appear to be the case with most models found in the literature, e.g. [2], except for the work of Ting *et al*. [5]. We consider only the diagonal disorder and ignore the off-diagonal disorder [7]. At any given interface, the roughness disorder is correlated, but we assume no correlation between different interfaces. This assumption was also used in Refs [2, 3, 5, 6]. For a single band calculation, our model reduces to that illustrated in Fig. 1. Figure 1 also illustrates the asymmetric roughness of the interfaces used in the calculations to model smooth normal interfaces and rough inverted interfaces [8]. The standard bulk Fröhlich Hamiltonian is used to model the polar optical phonons [9].

The current is obtained using non-equilibrium perturbation theory [10] which we have customized to meet the extreme demands of modeling high-bias, quantum electron transport with incoherent scattering through realistically long semiconductor devices [11]. The effect of the scattering is included through self-energy terms in an algorithm that appears to be quite similar to the multiple sequential scattering algorithm described by Roblin and Liou [3]. For both elastic scattering and inelastic scattering in the single electron approximation in which the Pauli exclusion is ignored, the self-consistent Born approximation results in an infinite continued fraction expansion for G^R and a power series expansion for $G^<$. Our algorithm allows one to truncate these expansions at any order and still conserve current [11–13]. In our calculations, the interface roughness is included to eighth order and the polar optical phonons to first order. In the language of Ref. [3], the interface

roughness is treated with eight sequential scattering events and the polar optical phonon scattering is treated with one sequential scattering event. For elastic scattering, Pauli exclusion plays no role in any type of Born approximation. For the inelastic scattering resulting from polar optical phonons, we use a single electron approximation so that the Pauli exclusion is ignored (current is still conserved) [14]. This should be a good approximation in the valley current since there is very little charge in the well. This approximation is also used in Refs [2, 3, 6].

The self energy resulting from interface roughness at layer j in a single band tight-binding model is

$$\Sigma^R_{j,j}(k) = x(1-x)\delta V^2 \frac{1}{A}\sum_{\boldsymbol{q}} |U_{\boldsymbol{k}-\boldsymbol{q}}|^2 G^R_{j,j}(q) \tag{1}$$

where $\boldsymbol{k}$ and $\boldsymbol{q}$ are momentum vectors in the plane of the interface, x is the fractional area covered by one of the cation species, A is the cross sectional area, and δV is the potential difference between the two bulk materials (in this case GaAs and AlAs). The spectral density, $|U_{\boldsymbol{k}}|^2$, is the Fourier transform of the autocorrelation function of the random cluster distribution. For a Kronecker delta autocorrelation, $|U_{\boldsymbol{k}}|^2 = a^2/2$ where a is the length of the conventional zincblende cubic cell, and we retrieve the expression for a single layer of alloy scattering. Traditionally, a Gaussian autocorrelation has been assumed [2, 3, 15] resulting in a momentum coupling of

$$|U_{\boldsymbol{k}}|^2 = \pi\Lambda^2 e^{-\Lambda^2 k^2/4}. \tag{2}$$

Recent STM work [16] indicates that an exponential autocorrelation may be more appropriate, resulting in a momentum coupling of

$$|U_{\boldsymbol{k}}|^2 = \frac{2\pi\Lambda^2}{[1+(k\Lambda)^2]^{3/2}} \tag{3}$$

where in Eqns (2) and (3) Λ is the correlation length.

The test structure that we simulate and experimentally measure is a GaAs/AlAs RTD with 19.2 nm intrinsic GaAs spacer layers, 3.4 nm AlAs barriers, and a 5.66 nm GaAs well. The n^+ GaAs contacts are Si doped 10^{18} cm^{-3}. All simulations and measurements are made at T = 4.2 K. In the simulations, we inject from and numerically integrate over all incident transverse momenta. This is in contrast to the work of Ref. [6] where numerical calculations were performed only for zero incident transverse momentum and the integration over incident transverse momenta was approximated analytically. Since the self energies are strongly dependent on the transverse momentum, this seems to be a questionable approximation especially for large Λ. In all of the simulations, we calculate the electrostatic potential from a self-consistent Schrödinger–Poisson calculation including a local density approximation for the exchange-correlation terms [17]. This calculation is performed with the incoherent scattering turned off. Once the potential is obtained, it is used for the calculation which includes the incoherent scattering. This is the same approach used in Refs [2, 3, 6]. Such an approach is reasonable for calculations of the valley current, since even with scattering assisted charging, there is relatively little charge in the well when the device is biased in the valley current region. However, it does not appear to be reasonable for current calculations near the peak current. The effect on the spectral function, $-2\mathrm{Im}\{G^R\}$, in the middle of the well of the interface roughness scattering with $\Lambda = 40$ nm is shown in Fig. (2). The bare resonance is Lorentzian with a full width at half maximum of 1 μeV. The dressed resonance has a split peak with a total width of 15 meV. Preliminary calculations indicate that the position, shape, and magnitude of the peak current is significantly altered if a full Hartree self-consistent calculation is performed which includes the effect of the scattering. For that reason, we will focus solely on the valley current.

Figure 3 shows a calculation of the valley current resulting from interface roughness using the exponential correlation model for five correlation lengths: 1, 5, 10, 40, and 100 nm. Initially, the valley current increases as Λ^2 corresponding to the numerator of Eqn (3). A cross over occurs for Λ between 5 and 10 nm and the

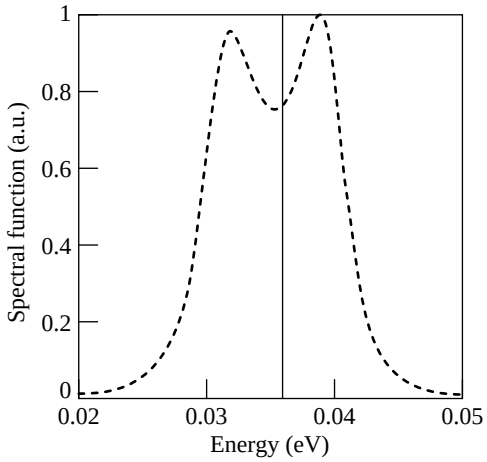

Fig. 2. Bare and dressed spectral functions in the centre of the well. The magnitude of each is normalized to a maximum of 1.0. The dressing results from exponential correlated interface roughness with $\Lambda = 40$ nm. (——), bare; (– – –), dressed.

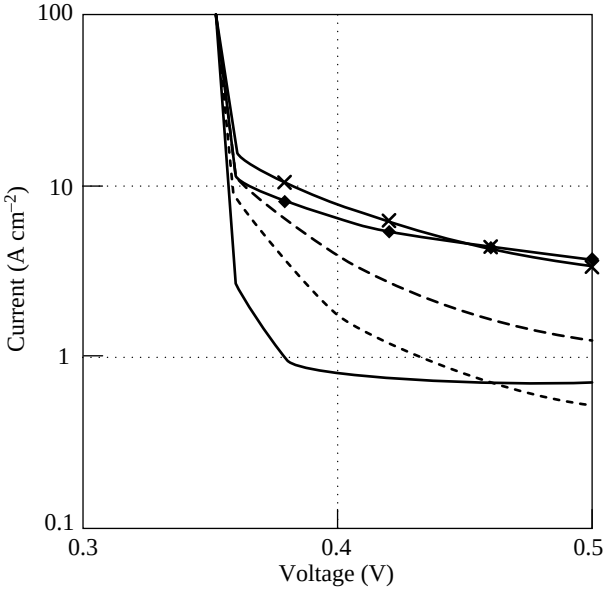

Fig. 3. Calculation of the valley current resulting from interface roughness scattering using the exponential correlation model for five correlation lengths: (——) 1; (–♦–), 5; (–×–) 10; (– – –), 40; and (· · · · · ·) 100 nm.

valley current begins to decrease with λ. This was also observed in Ref. [6]. As Λ increases, the term in the denominator of Eqn (3) eliminates large momentum transfer scattering causing the negative slope of the valley current.

The exponential and Gaussian correlation models are compared in Fig. 4 for three different correlation lengths: 1, 5, and 40 nm. For $\Lambda = 1$ nm, the current from the exponential model is approximately twice the current from the Gaussian model since for small Λ, $|U_{\boldsymbol{k}}|^2 \approx \pi\Lambda^2$ for the Gaussian model and $|U_{\boldsymbol{k}}|^2 \approx 2\pi\Lambda^2$ for the exponential model. For an intermediate Λ of 5 nm, the Gaussian model results in slightly more current

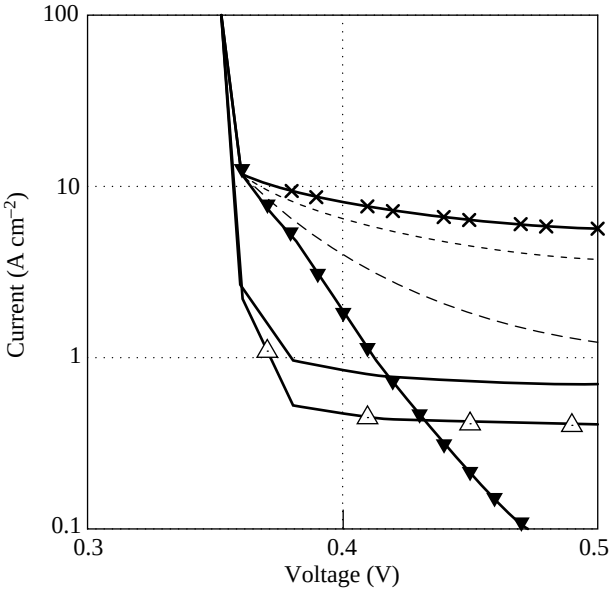

Fig. 4. Comparison of exponential and Gaussian correlation models for three correlation lengths: 1, 5, and 40 nm. (——), 1 nm exp; (–△–), 1 nm Gauss; (- - - - - -), 5 nm exp; (–×–), 5 nm Gauss; (– – –), 40 nm exp, (–▼–), 40 nm Gauss.

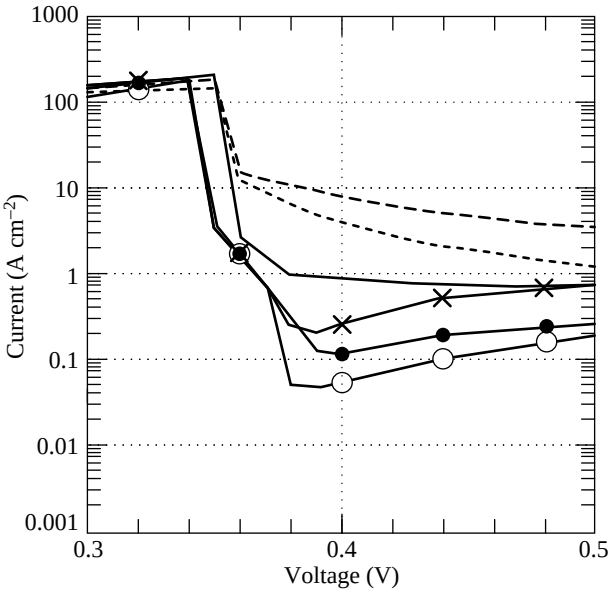

Fig. 5. Effect of roughness asymmetry using the exponential correlation model for three correlation lengths: 1, 10, and 40 nm. The asymmetry of the roughness is illustrated in Fig. 1. Forward and reverse bias I–Vs are plotted on the same quadrant. (——), 1 nm exp; (—○—), 1 nm exp reverse; (– – –), 10 nm exp; (–×–), 10 nm exp reverse; (- - - - - -), 40 nm exp; (—●—), 40 nm exp reverse.

than the exponential model. This is because $|U_{\boldsymbol{k}}|^2$ resulting from exponential correlation initially falls off faster than the Gaussian $|U_{\boldsymbol{k}}|^2$. However, the $|U_{\boldsymbol{k}}|^2$ resulting from exponential correlation has long tails so

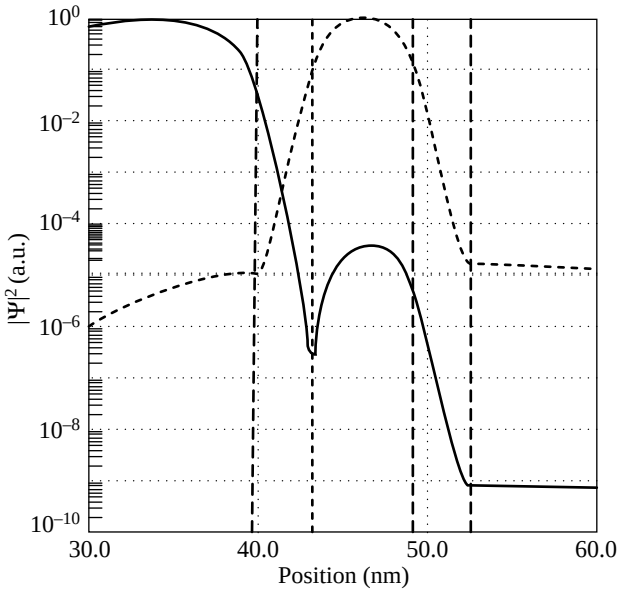

Fig. 6. Incident and resonant wavefunctions. The overlap at the first and third interfaces is larger than the overlap at the second and fourth interfaces. (– – –), barriers; (——), incident ψ; (- - - - - -), resonant ψ.

that for large Λ of 40 nm the exponential model results in more current than the Gaussian model. The current from the Gaussian model with $\Lambda = 40$ nm falls off nearly linearly on the semi-log plot which is exactly what one would expect from the Gaussian momentum coupling of Eqn (2).

The effect of roughness asymmetry is shown in Fig. 5 using the exponential correlation model for three different correlation lengths: 1, 10 and 40 nm. The direction of the incident electrons in forward and reverse bias with respect to the rough interfaces is shown in Fig. 1. For all correlation lengths, the valley current is significantly reduced in reverse bias when the injected electrons are incident on the smooth interfaces. The effect of asymmetric roughness on the current is easily understood by viewing the overlap of the incident and resonant wavefunctions in Fig. 6. The overlap at the first and third interfaces is much larger than the overlap at the second and fourth interfaces.

Finally, we turn to polar optical phonon scattering with $\Lambda = 6$ nm exponential interface roughness and compare with the experimental I–V in both forward and reverse bias in Fig. 7. Note from the discussion of Fig. 3 that $\Lambda = 6$ nm gives a maximum current contribution for interface roughness. The asymmetry seen in the experimental I–V is contrary to that expected from asymmetric interface roughness. We believe that it is the result of asymmetry of the dopant distributions in the two nominally intrinsic spacer layers. The current is calculated in forward and reverse bias with interface roughness alone and with interface roughness plus polar optical phonon scattering. The currents from the two different scattering mechanisms are essentially additive. Thus, the short dashed line in Fig. 7 is essentially the result of the polar optical phonon contribution which is significantly larger than the interface roughness contribution and appears to account for the majority of the valley current.

In summary, we have studied three aspects of interface roughness, different correlation lengths, the Gaussian and exponential correlation models, and roughness asymmetry, and shown how they affect the valley current of an RTD. A comparison of the calculated I–V with experimental data indicates that the valley current is dominated by polar optical phonon scattering.

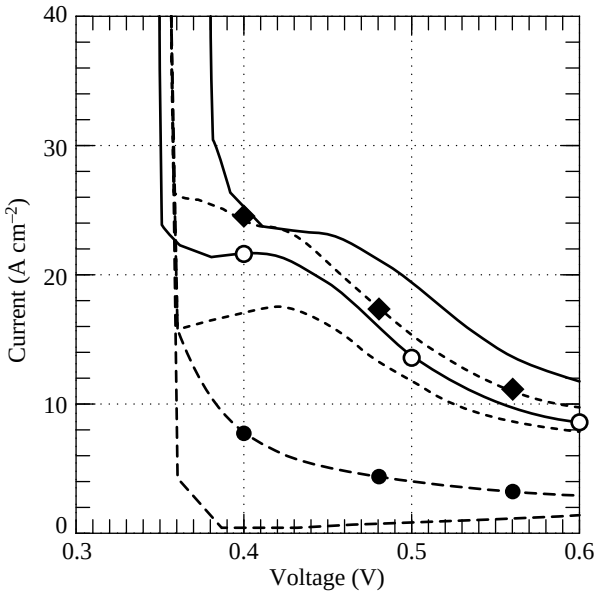

Fig. 7. Forward and reverse bias I–Vs (plotted on the same quadrant) from experimental data, calculations with 6 nm exponential asymmetric roughness, and calculations with the same 6 nm roughness plus polar optical phonon scattering. (——), Expt. reverse; (—○—) expt forward; (– – –), IR reverse; (—●—), IR forward; (- - - - - -), POPs reverse; (—◆—), POPs forward.

References

[1] The references cited in [2–5] provide a good overview of the literature.
[2] F. Chevoir and B. Vinter, Phys. Rev. B **47**, 7260 (1993).
[3] P. Roblin and W. Liou, Phys. Rev. B **46**, 2416 (1993).
[4] R. Lake and S. Datta, Phys. Rev. B **45**, 6670 (1992).
[5] D. Z. Y. Ting, S. K. Kirby and T. C. McGill, Appl. Phys. Lett. **64**, 2004 (1994).
[6] P. Roblin, R. C. Potter and A. Fathimulla, J. Appl. Phys. **79**, 2502 (1996).
[7] R. J. Lempert, K. C. Hass and H. Ehrenreich, Phys. Rev. B **36**, 1111 (1987).
[8] M. Tanaka and H. Sakaki, J. Crystal Growth **81**, 153 (1987).
[9] H. Fröhlich, Proc. R. Soc. London, Ser. A **160**, 230 (1937).
[10] D. C. Langreth, *Linear and Non-Linear Electron Transport in Solids*, NATO ASI series, vol. 17, edited by J. T. Devreese and E. van Doren, Plenum Press, New York: p. 3 (1976).
[11] R. Lake, G. Klimeck, R. C. Bowen and D. Jovanovic, in *The Theory of Single and Multi-Band Modeling of Wide Cross-Sectional Area, Steady-State, High-Bias Quantum Devices* (unpublished).
[12] R. Lake, in *Proceedings of the Third International Workshop on Computational Electronics*, Portland, OR, May 18–20: p. 239 (1994).
[13] R. Lake, in *Quantum Transport in Ultrasmall Devices*, NATO ASI Series, vol. 342, edited by D. K. Ferry, H. L. Grubin, C. Jacoboni and A. P. Jauho, Plenum Press, New York: p. 521 (1995).
[14] P. Hyldgaard, S. Hershfield, J. H. Davies and J. W. Wilkins, Ann. Phys. **236**, 1 (1994).
[15] T. Ando, A. B. Fowler and F. Stern, Rev. Mod. Phys. **54**, 437 (1982).
[16] R. M. Feenstra *et al*. Phys. Rev. Lett. **72**, 2749 (1994).
[17] E. Gawlinski, T. Dzurak and R. A. Tahir-Kheli, J. Appl. Phys. **72**, 3562 (1992).